PLEASE CITE THIS ARTICLE AS DOI: 10.1063/5.0211276

Amber free energy tools: Interoperable software for free energy simulations using generalized quantum mechanical/molecular mechanical and machine learning potentials

Yujun Tao,[†] Timothy J. Giese,[†] Şölen Ekesan,[†] Jinzhe Zeng,[†] Bálint Aradi,[‡] Ben Hourahine,[¶] Hasan Metin Aktulga,[§] Andreas Götz,^{||} Kenneth M. Merz, Jr.,[§] and Darrin M. York^{*,†}

Laboratory for Biomolecular Simulation Research, Institute for Quantitative Biomedicine and Department of Chemistry and Chemical Biology, Rutgers University, Piscataway, NJ 08854, USA, Bremen Center for Comp. Mater. Sci., University of Bremen, D-28334 Bremen, Germany, SUPA, Department of Physics, University of Strathclyde, Glasgow G4 0NG, United Kingdom, Department of Chemistry, Michigan State University, East Lansing, MI 48824, USA, and San Diego Supercomputer Center, University of California San Diego, La Jolla, CA 92093, USA

E-mail: Darrin.York@rutgers.edu

^{*}To whom correspondence should be addressed

[†]Laboratory for Biomolecular Simulation Research, Institute for Quantitative Biomedicine and Department of Chemistry and Chemical Biology, Rutgers University, Piscataway, NJ 08854, USA

[‡]Bremen Center for Comp. Mater. Sci., University of Bremen, D-28334 Bremen, Germany

SUPA, Department of Physics, University of Strathclyde, Glasgow G4 0NG, United Kingdom

[§]Department of Chemistry, Michigan State University, East Lansing, MI 48824, USA

San Diego Supercomputer Center, University of California San Diego, La Jolla, CA 92093, USA

PLEASE CITE THIS ARTICLE AS DOI: 10.1063/5.0211276

ABSTRACT: We report the development and testing of new integrated cyberinfrastructure for performing free energy simulations with generalized hybrid quantum mechanical/molecular mechanical (QM/MM) and machine learning potentials (MLPs) in Amber. The Sander molecular dynamics program has been extended to leverage fast, density-functional tightbinding models implemented in the DFTB+ and xTB packages, and an interface to the DeePMD-kit software enables use of machine-learning potentials (MLPs). The software is integrated through application program interfaces that circumvent the need to perform "system calls" and enables the incorporation of long-range Ewald electrostatics into the external software's self-consistent field procedure. The infrastructure provides access to QM/MM models that may serve as the foundation for QM/MM- Δ MLP potentials which supplement the semiempirical QM/MM model with a MLP correction trained to reproduce ab initio QM/MM energies and forces. Efficient optimization of minimum free energy pathways is enabled through a new surface-accelerated finite-temperature string method implemented in the FE-ToolKit package. Furthermore, we interfaced Sander with the i-PI software by implementing the socket communication protocol used in the i-PI client-server model. The new interface with i-PI allows for the treatment of nuclear quantum effects with semiempirical QM/MM-ΔMLP models. The modular interoperable software is demonstrated on proton transfer reactions in guanine-thymine mispairs in DNA. The current work represents a considerable advance in the development of modular software for performing free energy simulations of chemical reactions that are important in a wide range of applications.

PLEASE CITE THIS ARTICLE AS DOI: 10.1063/5.0211276

Introduction

Free energy simulations are used to study a wide range of reactive chemical processes in the condensed phase. 1,2 Calculation of multi-dimensional free energy surfaces 3,4 (FES) and minimum free energy paths⁵⁻⁹ (MFEP) can be used to predict mechanism. The insight gained by these predictions can aid in the interpretation of experimental data, guide new experiments, and ultimately inform the design of new technology. Ab initio quantum mechanical models can provide high accuracy in these simulations; however, their computational cost can severely limit the size of the quantum system and/or the degree of sampling that can be realized. This limitation is further amplified if path integral molecular dynamics (PIMD)¹⁰⁻¹⁵ is required to introduce nuclear quantum effects, as these simulations are even more computationally intensive.

An attractive alternative to ab initio QM/MM simulation is the design quantum mechanical force fields 2,16,17 and machine learning models. $^{18-23}$ Of particular relevance to the current work is the development of QM/MM-ΔMLP models, whereby the energies and forces of a fast, approximate QM model are corrected with a machine-learning potential. ^{20,24–30} These models have the potential to offer the computational efficiency needed to address complex chemical mechanisms that require sampling of high-dimensional free energy surfaces, while providing accuracy comparable to high level QM methods. A barrier to progress in the development and validation of such methods is their availability in flexible software packages that enable a wide range of applications in the condensed phase.

The purpose of the present work is to report the development and testing of interoperable simulation software in Amber for performing free energy simulations (including PIMD) with $QM/MM-\Delta MLP$ models. A list of software components is itemized in Table 1 and Figure 1 illustrates their interoperation. Specifically, we have extended the QM/MM capabilities of the Sander molecular dynamics program by introducing interfaces to the DFTB+42 and xTB³⁸⁻⁴¹ semiempirical QM packages. This enables access to a wide range of powerful new density-functional tight-binding models with enabled dispersion and hydrogen bond-

This is the author's peer reviewed, accepted manuscript. However, the online version of record will be different from this version once it has been copyedited and typeset PLEASE CITE THIS ARTICLE AS DOI: 10.1063/5.0211276

External Packages AMBER FE Engine FE-ToolKit **Alchemical Potential of Mean Force** (thermodynamic) (kinetic/mechanistic) **PLUMED Book-ending** FE surface Blue = distributed in Interoperability: Enhanced sampling, AMBERTools: PBC/PME generalized ensembles Green = interfaced electrostatics software **Force Field Potentials** iPI MM MM SQM **xTB** QM/MM-AMLP semi empirical DFTB+ QM QUICK ab initio **HFDF** DeePMD-kit **AMLP** DP

Figure 1: Interoperable software in Amber for conducting free energy simulations in the condensed phase with $QM/MM-\Delta MLP$ models. Amber-colored rectangle indicates Sander program with general internal components encircled by blue. Arrows indicate calling sequence. Green ovals are external software packages not distributed with Amber/AmberTools, whereas blue ovals indicate new cyberinfrastructure distributed with Amber. The program names and functionality are described in Table 1.

This is the author's peer reviewed, accepted manuscript. However, the online version of record will be different from this version once it has been copyedited and typeset PLEASE CITE THIS ARTICLE AS DOI: 10.1063/5.0211276

Table 1: Summary of program acronyms and functionality.

| D | |
|------------|---|
| Program | Function |
| Sander | A molecular dynamics program with support for QM/MM potentials. ³¹ |
| QUICK | A GPU-accelerated ab initio QM program. 32–36 |
| HFDF | An ab initio QM program optimized for large memory CPU machines. ³⁷ |
| хТВ | A semiempirical tight-binding program that implements the GFN1-xTB and GFN2-xTB models. $^{38-41}$ |
| DFTB+ | A self-consistent charge density functional tight binding program that |
| | implements the DFTB2 and DFTB3 methods and various dispersion models. $^{\rm 42}$ |
| DeePMD-kit | A machine learning library for performing deep potential training and inference based on the TensorFlow platform. 43–45 |
| i-PI | A program for performing path integral molecular dynamics. 46 |
| PLUMED | A library that implements enhanced-sampling algorithms, collective |
| | variable definitions, and biasing potentials to calculate free energy surfaces. 47,48 |
| WESTPA | An interoperable, scalable software package for |
| | weighted ensemble simulation and analysis. 49,50 |
| FE-ToolKit | A collection of programs used to analyze alchemical free energy |
| | simulations and umbrella window sampling. ⁵¹ |

ing corrections for use in condensed phase QM/MM simulations with rigorous long-ranged electrostatics under periodic boundary conditions. ^{37,52–54}Furthermore, we incorporated the DeePMD-kit software 43-45 into Sander 31 to evaluate new machine-learning potentials. Path integral molecular dynamics (PIMD) have been enabled through a new interface with the i-PI software. 46 Finally, a recently developed surface-accelerated finite-temperature string method⁹ has been incorporated into the FE-ToolKit software⁵¹ (distributed within Amber-Tools³¹) to locate minimum free energy paths.

The Methods section describes the interfaces between Sander, the DFTB+ and xTB semiempirical packages, the DeePMD-kit software, and i-PI. The nature of the QM/MM interactions and the incorporation of Ewald electrostatics within the self-consistent field (SCF) procedures are discussed. We demonstrate the features of the software framework through an example application that examines guanine-thymine mispair tautomerization reactions in B-DNA. These mispairs are enabled by formation of rare tautomer forms, and have been implicated in the formation of mutations in DNA replication and translation. ^{55,56} The

PLEASE CITE THIS ARTICLE AS DOI: 10.1063/5.0211276

Results and Discussion section begins with a validation of the implementation by demonstrating QM/MM and QM/MM- Δ MLP energy conservation in simulations performed in the microcanonical ensemble. We then compare free energy profiles generated from ab initio, semiempirical, and Δ MLP-corrected semiempirical methods obtained from QM/MM umbrella sampling. Finally, we perform QM/MM umbrella sampling with PIMD to explore how nuclear quantum effects alter the profiles.

Methods

The QM/MM- Δ MLP force fields are supplement the QM/MM energy with a nonelectrostatic correction, $E_{\rm ML}(\{{\bf r}\})$, where $\{{\bf r}\}$ is the 3N array of atomic positions.

$$E_{\text{QM/MM-}\Delta\text{MLP}} = E_{\text{MM}}(\{\mathbf{r}\}) + E_{\text{QM}}(\{\mathbf{r}\}; \mathbf{P}) + E_{\text{QM/MM}}(\{\mathbf{r}\}; \mathbf{P}) + E_{\text{ML}}(\{\mathbf{r}\})$$
(1)

 $E_{\rm MM}$ and $E_{\rm QM}$ are the MM and QM contributions to the energy, and $E_{\rm QM/MM}$ is their interaction. $E_{\rm ML}$ is the machine learning correction (referred to as a machine learning potential correction, Δ MLP). $E_{\rm QM}$ and $E_{\rm QM/MM}$ depend on the single particle density matrix, **P**. In the present work, we incorporated the DFTB+ and xTB packages into Sander for calculating E_{QM} , and the interface to DeePMD-kit is used to evaluate E_{ML} . The details of the implementation, and a description of the QM/MM interactions are discussed below.

Sander interface with DFTB+ and xTB

The DFTB+ and xTB source codes ^{57,58} are not distributed with AmberTools, but they can be downloaded and compiled as standalone applications and/or software libraries to be used in other applications. In our implementation, we directly link the DFTB+ and xTB libraries with the Sander executable during compilation. Unlike many of the other QM/MM interfaces supported by Sander, this strategy circumvents the cost associated with writing an input file for the external QM program, executing the external program via a system call, and

PLEASE CITE THIS ARTICLE AS DOI: 10.1063/5.0211276

reading the external program's output file at each molecular dynamics step. Instead, Sander directly interacts with DFTB+ and xTB via function calls. Furthermore, this allows us to incorporate variational long-range Ewald electrostatics into their SCF procedures. 37,52–54 Detailed instructions for configuring Sander with DFTB+ and xTB support are provided in the AmberTools 2024 user manual.

The QM/MM interaction is performed with electrostatic embedding.

$$E_{\text{QM/MM}} = E_{\text{QM/MM,LJ}} + \sum_{b \in \text{MM}} ' \int \int \frac{q_{\text{QM}}(\mathbf{r}')q_b(\mathbf{r} - \mathbf{r}_b)}{|\mathbf{r} - \mathbf{r}'|} d^3r d^3r'$$

$$+ \sum_{a \in \text{QM}} q_a \left(\Delta \phi_{\text{MM}}(\mathbf{r}_a) + \frac{1}{2} \Delta \phi_{\text{QM}}(\mathbf{r}_a) \right)$$
(2)

 $E_{\rm QM/MM,LJ}$ is the Lennard-Jones interaction between the QM and MM atoms. The second term is the electrostatic interaction between the QM charge density (determined from the density matrix), $q_{\text{QM}}(\mathbf{r})$, and the field of nearby MM charges $q_b(\mathbf{r} - \mathbf{r}_b)$. The primed summation denotes that only those MM atoms within a cutoff of the QM region are included. The last term accounts for the long-range electrostatic interactions. The QM charge density is modeled by Mulliken charges, q_a , $\Delta\phi_{\rm MM}(\mathbf{r}_a)$ is the electrostatic potential caused by all MM atoms outside of the cutoff, and $\Delta\phi_{\rm QM}(\mathbf{r}_a)$ the interaction between the QM region and its periodic images.

$$\Delta \phi_{\text{MM}}(\mathbf{r}_{a}) = \text{Re} \sum_{\mathbf{k} \neq 0} \frac{4\pi}{k^{2} V} e^{i\mathbf{k}^{T} \cdot \mathbf{r}_{a} - \frac{k^{2}}{4\beta^{2}}} \sum_{b \in \text{MM}} q_{b} e^{-i\mathbf{k}^{T} \cdot \mathbf{r}_{b}}$$
$$- \sum_{b \in \text{MM}} \frac{q_{b} \operatorname{erf}(\beta r_{ab})}{r_{ab}} - \frac{\pi Q_{\text{MM}}}{\beta^{2} V}$$
(3)

$$\Delta \phi_{\text{QM}}(\mathbf{r}_{a}) = \text{Re} \sum_{\mathbf{k} \neq 0} \frac{4\pi}{k^{2}V} e^{i\mathbf{k}^{T} \cdot \mathbf{r}_{a} - \frac{k^{2}}{4\beta^{2}}} \sum_{b \in \text{QM}} q_{b} e^{-i\mathbf{k}^{T} \cdot \mathbf{r}_{b}}$$
$$- \sum_{b \in \text{QM}} \frac{q_{b} \operatorname{erf}(\beta r_{ab})}{r_{ab}} - \frac{\pi Q_{\text{QM}}}{\beta^{2}V}$$
(4)

PLEASE CITE THIS ARTICLE AS DOI: 10.1063/5.0211276

The first term in eqs. 3 and 4 is the reciprocal space potential of the MM and QM charge densities, respectively. V is the volume of the unit cell, β is the Ewald coefficient, **k** is the angular wave number of the plane wave, and $Q_{\rm MM}$ and $Q_{\rm QM}$ are the net charge of the MM and QM regions. The second term in eqs. 3 and 4 is a real-space correction that removes the potential caused by the nearby Ewald Gaussian functions. The third term in eqs. 3 and 4 is a neutralizing uniform background correction for charged systems. The MM energy, $E_{\mathrm{MM}}(\{\mathbf{r}\})$ contains an analogous background correction $-\pi Q_{\mathrm{MM}}^2/(2\beta^2 V)$, such that the net correction for the entire system is $-\pi (Q_{\text{MM}} + Q_{\text{QM}})^2/(2\beta^2 V)$.

The Sander program is responsible for calculating $E_{\rm MM}$, $E_{\rm MM,LJ}$, $\Delta\phi_{\rm MM}$, and $\Delta\phi_{\rm QM}$. The DFTB+ and xTB libraries are responsible for calculating E_{QM} , q_a , and the second term in eq. 2. A similar separation of responsibilities occurs when calculating atomic forces. At each step of dynamics, Sander evaluates $\Delta \phi_{\rm MM}$ with the particle mesh Ewald (PME) method, ^{59,60} and it precomputes the exponentials appearing in eq. 4. The MM atoms are imaged around the QM region, and a list of MM atoms within a cutoff of any QM atom is generated. A SCF calculation is requested by providing the current set of QM atomic coordinates, and the locations, charges, and "hardness" values of the nearby MM atoms. The xTB software uses the hardness values to represent the nearby embedding charges as diffuse monopoles. For example, in GFN2-xTB, the second term in eq. 2 is given by eq. 5, where s indexes the atomic orbital shells, and q_s is a shell-resolved partial charge.

$$\sum_{b \in \text{MM}}' \int \int \frac{q_{\text{QM}}(\mathbf{r}')q_b(\mathbf{r} - \mathbf{r}_b)}{|\mathbf{r} - \mathbf{r}'|} d^3r d^3r' \approx \sum_{b \in \text{MM}}' \sum_{a \in \text{QM}} \sum_{s \in a} \frac{q_s q_b}{\sqrt{r_{ab}^2 + \left\lceil \frac{\eta_s + \eta_b}{2} \right\rceil^{-2}}}$$
(5)

In the present work, we assign all MM atoms the hardness of hydrogen. The Sander interface with DFTB+ currently treats the MM atoms as point charges; however, this can be generalized in a similar fashion in the future.

The interfaces to both QM packages take advantage of object oriented features of the Fortran 2008 programming language to communicate the variational contribution of the

PLEASE CITE THIS ARTICLE AS DOI: 10.1063/5.0211276

long-range electrostatics within the SCF procedure. The DFTB+ interface with Sander is contained in the file dftbplus_module.F90 located in the Sander source directory of the AmberTools 2024 package. The interface creates a child class that inherits from the TODepExtPotGen data structure provided by the DFTB+ software. ⁵⁷ This class was specifically designed by the DFTB+ developers to include charge-dependent external potential corrections. The xTB interface with Sander is similarly contained in the file xtb module.F90 within the Sander source directory. The xTB interface inherits from the TSolvation structure defined within the xTB software. 58 xTB normally uses this class to interact the QM region with an implicit solvent model. In both interfaces, the child class redefines the parent class methods to evaluate the last term in eq. 2 and the "shift" in the atom potentials: $\Delta \phi_{\mathrm{MM}}(\mathbf{r}_a) + \Delta \phi_{\mathrm{QM}}(\mathbf{r}_a).$

One enables QM/MM calculations by setting ifqnt=1 in the Sander input file, which will cause the options in the agmmm Fortran namelist to be read. Setting the option qm_theory='DFTBPLUS' or qm_theory='XTB' will read the interface-specific options in the &dftbplus or &xtb namelists, respectively. Additional details are described in the upcoming AmberTools 2024 documentation, due to be released in the spring of 2024.

Sander interface with DeePMD-kit

The design of the DeePMD-kit interface 43-45 with the Sander program 31 is heavily influenced by the development of QM/MM- Δ MLP potentials. ^{20,21,61-64} In the Sander input file, the user makes a selection of atoms to be corrected with a MLP. In the context of evaluating a QM/MM-ΔMLP, the MLP selection is the set of atoms in the QM region. One must also provide the name of the file containing the DeePMD-kit neural network definition and parameters. The Deep-Potential Range-Corrected model (DPRc)²⁰ corrects the interactions between the QM atoms and the interactions between the QM and nearby MM atoms in a manner that conserves energy. That is to say, the MLP correction to the QM/MM interactions smoothly approaches zero as the MM atom reaches a specified cutoff distance. When

PLEASE CITE THIS ARTICLE AS DOI: 10.1063/5.0211276

using a DPRc model, the Sander input file must also specify the MLP cutoff for the QM/MM interactions. Previous parametrizations of DPRc-based MLP models have used a 6 Å cutoff, which is also used in the present work. At each step of dynamics, Sander will request the MLP energy and forces from DeePMD-kit by providing the position and "type" of each QM and (optionally) nearby MM atoms. A QM atom type is its 2-character element symbol, whereas the MM atom type – from the perspective of DeePMD-kit – is the element symbol prefixed with the letter "m". This strategy allows the neural network to correct a QM/QM interaction differently than a QM/MM interaction.

The DPRc energy is the sum of atomic contributions, E_i ,

$$E_{\text{DPRc}} = \sum_{i=1}^{N} E_i(\mathbf{r}_i, \{\mathbf{r}_j\}_{j \in n(i)})$$
(6)

where N is the number of atoms, \mathbf{r}_i is the location of atom i, and n(i) denotes the set of neighboring atoms (i.e., atoms within the DPRc cutoff radius). The expressions for the E_i values from the neural network can be found elsewhere. ^{20,21} The atomic decomposition of DPRc model is readily amenable to parallel calculation. The DPRc contribution to the energy is activated by setting the idprc=1 option within the Sander input &dprc Fortran namelist.

As written, the DPRc application programming interface is specific to DeePMD-kit because it instantiates software objects defined within the DeePMD-kit library. Many emerging MLPs, such as allegro⁶⁵ and mace, ⁶⁶ are based on the PyTorch framework. ⁶⁷ We are currently developing a generic Sander/PyTorch QM/MM-ΔMLP interface to evaluate these models.

Sander interface with i-PI

The i-PI software 46 is a standalone molecular dynamics program that supports state-of-theart path integral sampling, 68 including the PIGLET thermostat, which has been shown to

PLEASE CITE THIS ARTICLE AS DOI: 10.1063/5.0211276

dramatically reduce the expense of computing the quantum kinetic energy. ^{69,70} The path integral dynamics is performed with a ring polymer Hamiltonian, consisting of several replicas (beads) that are harmonically restrained in series. At each time step, the potential energy of each bead must be computed; however, these calculations are independent and can be performed in parallel. The i-PI software defines a client-server communication protocol to evaluate the potential energy with external driver programs. We have implemented the "internet socket" variation of the protocol, where multiple instances of Sander can be launched on different computers. When launching a Sander instance, one must provide the hostname (internet protocol address) and port number used for interprocess communication. These quantities are specified as command-line arguments -host and -port, respectively. Furthermore, the Sander input file must set the option imin=7, which causes the program to wait for communication from the server process.

Free energy profiles of tautomer reactions from classical molecular dynamics

We prepared a B-form DNA system (PDB ID: 113D)⁷¹ to demonstrate the functionality of the new software infrastructure. The B-DNA crystal structure⁷¹ has drawn interest due to the presence of two G-T wobble pair mismatches 55,72,73 which could give rise to errors in replication ^{74,75} and translation. ⁷⁶ This subsequently led to computational investigation of G-T tautomerization reactions with QM/MM.⁵⁶

In the present work, we explore tautomerization reactions involving residues G4 and T21. The B-DNA system consists of 762 solute atoms solvated by 5151 waters in a truncated octahedron with 59.3 Å real-space lattice vectors lengths. A total of 13 Cl⁻ and 35 Na⁺ ions were added to neutralize the charge and achieve a 0.14 M ion concentration. The system was prepared using an elaborate 15-step procedure described in Ref. 77 using a MM potential. The preparation procedure involves geometry optimization, heating, solvent annealing, and equilibration of the system density while restraining solute heavy atoms.

PLEASE CITE THIS ARTICLE AS DOI: 10.1063/5.0211276

Over the course of the equilibration procedure, the solute restraints are gradually reduced. In total, this procedure involved 6.2 ns and 2.6 ns of simulation in the *NVT* and *NPT* ensembles, respectively, using a 1 fs time step. The system was then equilibrated for an additional 100 ns in the *NPT* ensemble. The temperature was maintained at 298 K with a Langevin thermostat⁷⁸ (5.0 ps⁻¹ collision frequency) and the density was equilibrated at 1 atm using the Berendsen isotropic barostat. The MM potential modeled the DNA with the OL15 force field,⁷⁹ and the solvent environment was modeled with SPC/Fw waters⁸⁰ and the Li *et al.* ion parameters.⁸¹ Electrostatics were calculated with the particle mesh Ewald method^{59,60} using 10 Å real-space cutoffs, a 1 Å reciprocal space grid spacing, and tinfoil boundary conditions.

Free energy profiles of the tautomeric reactions depicted in Figure 3 were calculated from QM/MM umbrella sampling using a variety of ab initio and semiempirical methods. The reactions are decomposed into 3 steps connecting 3 tautomeric forms. The "wGT" state corresponds to the G-T wobble base pair in which the T21:N3 position is protonated. The "GT*" state is a tautomer in which the T21:H3 proton is covalent bonded to the T21:O4 position. Similarly, the "G*T" state is a tautomer in which the H3 proton is bound to the G4:06. The 3 steps involve the proton displacement between these states: $wGT \rightarrow GT^*$, $GT^* \rightarrow G^*T$, $G^*T \rightarrow wGT$. The QM/MM methods compared in this work are: PBE0/6-31G*, GFN2-xTB, 41 DFTB3-D3 DFTB3-D4(2b), DFTB3-D4(3b), and AM1/d. 82-84 The DFTB3-D3 model applies Grimme's D3 dispersion correction 85,86 to the DFTB3/3ob Hamiltonian. 87,88 Similarly, the DFTB3-D4(2b) and DFTB3-D4(3b) models supplement the DFTB/3ob method with the D4 dispersion model.⁸⁹ The DFTB3-D4(3b) method includes a 3-body contribution to the dispersion, whereas DFTB3-D4(2b) is limited to 2-body contributions. Furthermore, we parametrized a reaction-specific DPRc correction for the AM1/d model (described in the next section), which will be denoted AM1/d+ML. The QM region consists of 51 atoms (the nucleobase and sugar of G4 and T21), and it has a net neutral charge. The minimum free energy path of each step was independently optimized

PLEASE CITE THIS ARTICLE AS DOI: 10.1063/5.0211276

for every QM/MM model. The optimizations were performed with the surface-accelerated finite temperature string method⁹ in the space of 5 reaction coordinates. The reaction coordinates are distance differences meant to represent the transfer of H3 proton and the relative displacement of the hydrogen bond pattern: $\xi_1 = R_{\text{N3-H3}} - R_{\text{O6-H3}}, \, \xi_2 = R_{\text{O6-H3}} - R_{\text{O4-H3}},$ $\xi_3 = R_{\text{N1-H1}} - R_{\text{N3-H1}}, \, \xi_4 = R_{\text{N1-O2}} - R_{\text{N2-O2}}, \, \xi_5 = R_{\text{N2-O2}} - R_{\text{N1-N3}}.$ All umbrella sampling described in this work used 200 kcal mol^{-1} Å⁻² force constants for each reaction coordinate. The string method began from an initial guess that linearly interpolated the reaction coordinates between the step's reactant and product states. Each string was sampled with 32 umbrella windows. The initial configurations of each window were sequentially prepared, starting from the reactant state. The QM/MM structure of each window was optimized for 1000 steps of conjugate gradient minimization. The temperature was gradually raised from 0 K to 298 K over the course of 40 ps, and an additional 10 ps of QM/MM umbrella sampling was performed in the NVT ensemble. 50 iterations of the string method were performed with 4 ps/window/iteration of sampling and a 1 fs time step. Production sampling of the final path was performed for 25 ps, and each production simulation was repeated 4 times with different thermostat random number seeds. The reaction coordinate values were recorded every 10 fs, and the aggregate sampling from all 3 reaction steps were analyzed with the multistate Bennett's acceptance ratio (MBAR) method⁹⁰ implemented in the ndfes software 4,51 to produce 5-dimensional free energy surfaces. The profiles presented in the manuscript are the free energies along the minimum free energy path. The PBE0/6-31G* simulations is very expensive in relation to the other models. In this case, only 10 iterations of the string method were performed, starting from the optimized AM1/d path. Each string was sampled for 2 ps/window/iteration, and 4 sets of production simulations were run for 10 ps/window/trial with a 1 fs time step. The ab initio QM/MM electrostatics were calculated with the ambient-potential composite Ewald method³⁷ using a 10 Å real-space cutoff, 1 Å reciprocal space grid spacing, and tinfoil boundary conditions.

PLEASE CITE THIS ARTICLE AS DOI: 10.1063/5.0211276

Free energy profiles of tautomer reactions from path integral molecular dynamics

We recalculated the free energy profiles from path integral molecular dynamics (PIMD) umbrella sampling performed with the new interface to the i-PI software. ⁶⁸ The profiles generated from classical and path integral dynamics are compared to explore how nuclear quantum effects change the free energy predictions. The PIMD dynamical motion was propagated with 6 beads (replicas) at a 0.25 fs timestep at 298 K using the PIGLET quantum thermostat: ^{69,91} therefore, up to 6 Sander instances can be launched. The parameters for the PIGLET thermostat were taken from the GLE4MD website. 92,93 The parameters were chosen to reproduce the quantum fluctuations at 298 K and span a range of frequencies up to 4142 cm⁻¹. Each step's path was sampled with 32 umbrella windows using 200 kcal mol⁻¹ \mathring{A}^{-2} force constants. The PIMD restraint potentials were applied to the centroid positions (the bead-averaged positions) by making use of the i-PI interface to PLUMED. 47,48 PIMD umbrella sampling was performed at 32 windows positioned along the path previously optimized from the classical sampling. Each window was sampled for 2.5 ps, and repeated 4 times with different thermostat random number seeds. The reaction coordinate values were calculated from the centroid positions, and the free energy surface was generated from MBAR analysis of the aggregate sampling obtained from the 3 reaction steps.

$QM/MM-\Delta MLP$ model training

We demonstrate the new interface between Sander and DeePMD-kit by parametrizing a DPRc correction for the AM1/d-PhoT Hamiltonian. The architecture of the DPRc neural network was previously described in Ref. 94, and we have summarized the model in the Supporting Information for completeness. The AM1/d+ML neural network parameters were optimized with the DP-GEN software 95 to reproduce PBE0/6-31G* QM/MM energies and forces in the B-DNA system. The DPRc MLP corrects the interactions between the

PLEASE CITE THIS ARTICLE AS DOI: 10.1063/5.0211276

QM atoms, and the QM/MM interactions within a 6 Å cutoff. Four sets of neural network parameters were trained against 93617 samples extracted from the AM1/d-PhoT string calculations using the Adam stochastic optimizer with different random number seeds. 96 The parameter sets were then updated through 7 iterations of active learning. An active learning iteration consists of 3 steps: exploration, labeling, and retraining. The exploration step uses the current set of neural network parameters to perform $QM/MM+\Delta MLP$ umbrella sampling. For each saved sample, the energy and forces produced by the 4 parameter sets are compared; if the models disagree, then the sample is categorized as a "candidate". The "labeled" samples are a random selection of (up to) 2000 samples drawn from the pool of candidates. The energy and forces of labeled samples are recalculated with PBE0/6-31G* QM/MM and included as additional reference data within the next round of training. The active learning procedure terminates when 10% (or fewer) of the samples are selected for labeling.

Each active learning iteration sampled 1920 umbrella windows for 2 ps and saved 50 samples/simulation. These simulations correspond to the first 20 and 40 iterations of the finite temperature string method applied to the wGT \rightarrow GT* and GT* \rightarrow G*T reaction steps, respectively. A sample was made a candidate if the standard deviation in the MLP energy corrections was larger than 10^{-4} eV/atom or the standard deviation in the force correction exceeds 0.08 eV/Å for any atom. The active learning procedure terminated after 7 iterations, requiring a total of 9293 ab initio QM/MM evaluations. Neural network parameters were produced from 4 million steps of Adam stochastic optimization with a learning rate that exponentially decays from 10^{-3} to 5×10^{-8} . As previously described, production sampling of the B-DNA tautomeric reactions were simulated 4 times with different random number seeds. The AM1/d+ML production sampling was repeated with each of the 4 neural network parameter sets (1 trial/parameter set), and the results were averaged.

accepted manuscript. However, the online version of record will be different from this version once it has been copyedited and typeset

PLEASE CITE THIS ARTICLE AS DOI: 10.1063/5.0211276

This is the author's peer reviewed,

Results and Discussion

Validation tests: Force evaluation and energy conservation in NVE simulations

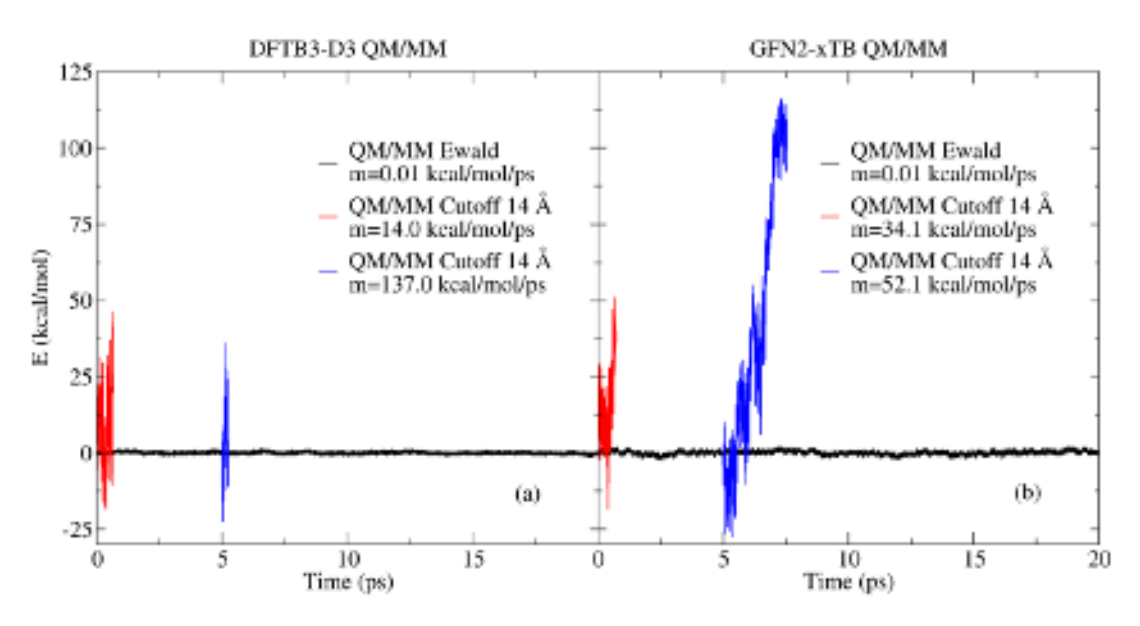


Figure 2: QM/MM energy conservation of B-DNA in the microcanonical ensemble. (a) DFTB3-D3 performed with Sander/DFTB+. (b) GFN2-xTB performed with Sander/xTB. All methods compute the MM/MM electrostatics with particle mesh Ewald. The QM/MM Ewald method similarly models the QM/QM and QM/MM electrostatics with Ewald. The QM/MM Cutoff 14 Å method truncates the QM/MM interactions beyond 14 Å, and long-range QM/QM interactions are ignored. The QM/MM Cutoff 14 Å simulations were repeated at different starting configurations taken from the QM/MM Ewald trajectory. The "m" values are the slope of the energy obtained from linear regression.

In this section, we validate the Sander interface with DFTB+ and xTB software by performing DFTB3-D3 and GFN2-xTB QM/MM simulations of the B-DNA system in the microcanonical ensemble and monitor the total energy. Energy conservation is achieved when the potential energy is smooth and the analytic atomic forces are numerically consistent with the potential energy gradients.

Figure 2 plots the total energy of the B-DNA reactant state as a function of time. The lines labeled "QM/MM Ewald" were simulated with Ewald electrostatics using 10~Å real-

PLEASE CITE THIS ARTICLE AS DOI: 10.1063/5.0211276

space cutoffs, whereas "QM/MM Cutoff 14 Å" truncates the QM/MM electrostatics at 14 Å(and it does not model the long-range QM/MM electrostatics). We ran the simulations with truncated electrostatics twice, starting from the GFN2-xTB (Ewald) or DFTB3-D3 (Ewald) configurations at times 0 ps and 5 ps. The "m" values are slopes of the energy from linear regression. Each simulation was performed for 20 ps using a 1 fs time step.

The QM/MM Ewald interface described in the methods section assumes that the shortrange QM/MM electrostatic interactions (the second term in eq. 2) behave like point monopoles at the real-space cutoff; the Ewald correction models the electrostatics outside of the cutoff from a point charge approximation. The short-range electrostatics (eq. 5) adopt the Mataga-Nihshimoto-Ohno-Klopman 97-99 damped Coulomb interaction model. This model mimics a point charge interaction at large distances.

Figure 2 suggests that the slight discrepancy between eq. 5 and point charge electrostatics is negligible when using a 10 Å real-space cutoff for both GFN2-xTB and DFTB3-D3. The energy conservation of GFN2-xTB is almost identical to DFTB3-D3 in DFBT+. Both models exhibit negligible energy drift over 20 ps (slopes 0.01 kcal/mol/ps). However, when the GFN2-xTB and DFTB3-D3 QM/MM electrostatics are truncated at 14 Å, large deviations in the total energy are encountered, and the self-consistent field procedure often fails to converge within a few picoseconds of simulation. Similar behavior has been illustrated elsewhere in validation tests that compare the stability of QM/MM simulations with and without longranged electrostatic interactions.³⁷

Free energy surfaces for guanine-thymine mispair tautomerization reactions

In this section, we examine free energy profiles of guanine-thymine mispair tautomerization reactions using a wide range of ab initio and semiempirical/DFTB QM/MM and QM/MM-ΔMLP models. Free energy surfaces (FESs) and minimum free energy paths (MFEPs) were

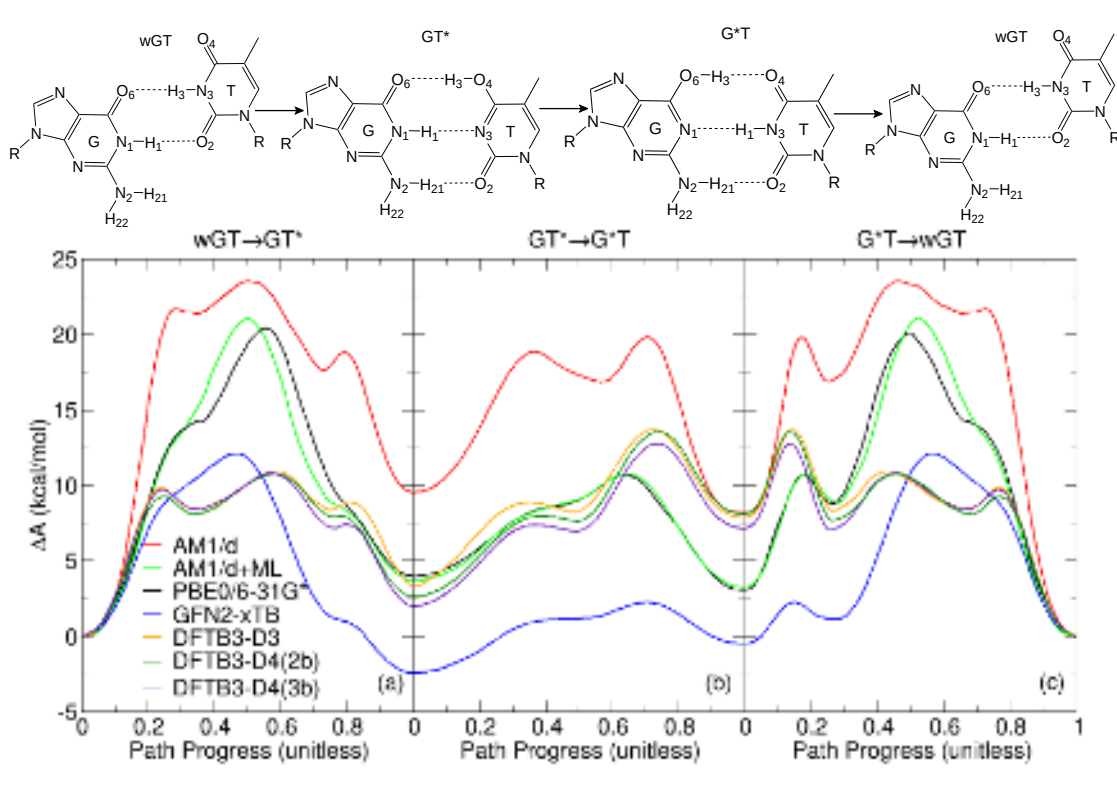


Figure 3: Helmholtz free energy profiles for guanine-thymine mispair tautomerization reactions using different *ab initio* and semiempirical/DFTB QM/MM and QM/MM- Δ MLP models performed in the canonical ensemble. (a) wGT \rightarrow GT*; (b) GT* \rightarrow G*T; (c) G*T \rightarrow wGT. "wGT" indicates a G-T wobble pair, and G* and T* are non-standard tautomer states of G and T, respectively, as indicated in the figure and described in the text.

PLEASE CITE THIS ARTICLE AS DOI: 10.1063/5.0211276

determined using the surface-accelerated string method⁹ with 5 different reaction coordinates as described in the Methods section. Figure 3 compares the 1D free energy profiles for the MFEPs for the following QM/MM models: PBE0/6-31G*, AM1/d, GFN2-xTB, DFTB3-D3, DFTB3-D4(2b), and DFTB3-D4(3b). PBE0/6-31G* is an ab initio QM/MM model, and it is approximately 500 times slower than the other semiempirical/DFTB QM/MM models for these systems. Several QM/MM models based on DFTB3 are available through the interface with DFTB+, and in particular the use of different dispersion models are examined. The notation "D3" and "D4" refers to the dispersion correction, (2b) and (3b) mean 2-body and 3-body interaction, respectively, as described in the Methods section. In addition, the GFN2xTB model is examined through an interface with the xTB package. The AM1/d model is an NDDO-based semiempirical Hamiltonian available within the SQM module of Sander. AM1/d also serves as the base QM model upon which the QM/MM- Δ MLP was developed (AM1/d+ML) through an interface with DeePMD-kit. $^{43-45}$ Neural network parameters were trained to reproduce PBE0/6-31G* QM/MM energies and forces. In this way, functionality for a wide range of QM/MM models is demonstrated, and their results compared.

The reaction itself is decomposed and presented in three steps that form a closed thermodynamic cycle as illustrated at the top of Figure 3. In the first step a G-T wobble pair (wGT) undergoes a coupled proton transfer/hydrogen bond register shift to a G-T* basepair where T* represents the thymine enol tautomer. In the second step of the reaction, the GT* undergoes a second proton transfer/hydrogen bond register shift to form a (G*)-T basepair where G* is the guanine enol tautomer. The third step of the reaction involves a coupled proton transfer/hydrogen bond register shift to return to the original GT wobble basepair.

It is immediately evident from Figure 3 that there are large variations in the free energy profiles for the various QM/MM models. Most notably, none of the semiempirical/DFTBbased QM/MM models closely reproduce the ab initio PBE0/6-31G* profile. The AM1/d model systematically overestimates the profile with respect to the wGT state, whereas the DFTB models underestimate the profiles with respect to the wGT state. The GFN2-xTB

PLEASE CITE THIS ARTICLE AS DOI: 10.1063/5.0211276

model, in this example, further predicts that the tautomer basepairs (GT* and G*T) are more favorable than the GT wobble (wGT) where the nucleobases are in their most stable tautomer keto forms.

Table 2 (top) lists values of key stationary points along the free energy profiles calculated with classical molecular dynamics shown in Figure 3 and compares them to experimentallyderived reference values. Overall, the ab initio PBE0/6-31G* QM/MM model does the best job at reproducing the experimentally derived values. The differences in ΔA are less than 1 kcal/mol, and the differences in ΔA^{\ddagger} are less than 3.5 kcal/mol. It should be noted that the comparison with experiment here is only approximate in the sense that the ΔA^{\ddagger} is only crudely approximated from the experimental rates using transition state theory with unit transmission coefficient. Taking the PBE0/6-31G* values as a high-level theoretical reference, it is clear that the other QM/MM models differ considerably. For example, the difference between PBE0/6-31G* and semiempirical/DFTB model wGT \rightarrow GT* ΔA^{\ddagger} values range from -6.4 to 5.6 kcal/mol. Only the machine-learning potential corrected model AM1/d+ML gives results that are close to the ab initio values. The ΔA and ΔA^{\ddagger} values agree with PBE0/6-31G* to within 0.5 and 0.8 kcal/mol, respectively. The AM1/d+ML QM/MM model is thus by far the closest agreement with the ab initio QM/MM model, despite the uncorrected AM1/d model having very large differences (maximum differences for ΔA and ΔA^{\ddagger} of 5.6 and 3.5 kcal/mol for ΔA and ΔA^{\ddagger} , respectively).

The main point of this section is to demonstrate that: 1. ab initio QM/MM simulations provide reasonable agreement with experimental results such that they can provide, at very high computational cost, a valuable molecular-level interpretation and can potentially be used for prediction; 2. existing semiempirical/DFTB models may not be able to accurately describe a chemical process that was outside the scope of their development; and 3. machine-learning potential corrections can provide an avenue toward improving efficient semiempirical/DFTB QM/MM models for specific applications. The software infrastructure reported here enables new types of QM/MM-ΔMLP models to be developed and applied in

PLEASE CITE THIS ARTICLE AS DOI: 10.1063/5.0211276

Amber to efficiently compute free energy surfaces and minimum free energy paths.

Nuclear quantum effects on guanine-thymine mispair tautomerization reactions

Table 2: Tautomer free energies and forward reaction barriers (kcal/mol) determined from classical and path integral molecular dynamics umbrella sampling.^a

| | wGT- | →GT* | GT*- | →G*T | G*T- | →wGT |
|------------------------------|-------------|-----------------------|--------------|-----------------------|-------------|-----------------------|
| Method | ΔA | ΔA^{\ddagger} | ΔA | ΔA^{\ddagger} | ΔA | ΔA^{\ddagger} |
| Expt. | 4.43 | 16.88 | -0.62 | 9.21 | -3.82 | ••• |
| | | | Classical MD | | | |
| PBE0/6-31G* | 3.97(0.04) | 20.41(0.05) | -0.91(0.03) | 6.72(0.05) | -3.06(0.04) | 17.02(0.05) |
| AM1/d | 9.54(0.04) | 23.51(0.06) | -1.36(0.03) | 10.26(0.03) | -8.16(0.04) | 15.36(0.04) |
| $\mathrm{AM1/d}\mathrm{+ML}$ | 3.67(0.07) | 21.01(0.07) | -0.43(0.07) | 7.06(0.07) | -3.24(0.07) | 17.78(0.07) |
| GFN2-xTB | -2.44(0.06) | 12.09(0.05) | 1.94(0.08) | 4.68(0.06) | 0.50(0.06) | 12.59(0.07) |
| DFTB3-D3 | 3.27(0.07) | 10.91(0.08) | 4.58(0.08) | 10.41(0.08) | -7.85(0.09) | 5.83(0.09) |
| DFTB3-D4 $(3b)$ | 2.01(0.10) | 10.81(0.09) | 5.13(0.12) | 10.75(0.09) | -7.14(0.12) | 5.59(0.11) |
| DFTB3-D4 $(2b)$ | 2.63(0.07) | 10.75(0.07) | 5.46(0.07) | 10.91(0.06) | -8.09(0.07) | 5.43(0.06) |
| | | | PIMD | | | |
| $\mathrm{AM1/d}$ | 7.98(0.07) | 21.87(0.08) | -1.46(0.08) | 6.90(0.06) | -6.51(0.09) | 15.41(0.08) |
| $\mathrm{AM1/d}\mathrm{+ML}$ | 3.48(0.03) | 20.65(0.04) | 0.26(0.03) | 4.21(0.08) | -3.75(0.04) | 16.88(0.04) |
| GFN2-xTB | -3.10(0.06) | 10.93(0.06) | 1.70(0.05) | 2.47(0.06) | 1.34(0.06) | 12.26(0.05) |
| DFTB3-D3 | 1.68(0.09) | 10.59(0.08) | 4.41(0.09) | 7.96(0.08) | -6.03(0.09) | 4.57(0.08) |
| DFTB3-D4 $(3b)$ | -0.57(0.08) | 9.99(0.10) | 5.12(0.07) | 8.12(0.07) | -4.55(0.07) | 5.44(0.09) |
| DFTB3-D4(2b) | 2.17(0.07) | 9.78(0.08) | 4.20(0.08) | 7.04(0.07) | -6.37(0.08) | 3.40(0.08) |

^a Each free energy profile was computed 4 times from independent sets of simulations. The tabulated values are the mean of the 4 trials. The numbers in parenthesis are the standard error of the mean. Experimental reference values were derived from rates measured in ref. 55, and free energy values approximated from transition state theory assuming a unit transmission coefficient.

In this section, we demonstrate the new interface with the i-PI software by calculating free energy profiles from PIMD simulation, as described in the Methods section. These calculations are considerably more computationally intensive (by roughly an order of magnitude, or more depending on the number of replicas used in the ring polymer Hamiltonian). Nonetheless, inclusion of nuclear quantum effects is important, especially for modeling chemical reactions that involve proton transfer events such as those presented here. Other recent

This is the author's peer reviewed,

accepted manuscript. However, the online version of record will be different from this version once it has been copyedited and typeset PLEASE CITE THIS ARTICLE AS DOI: 10.1063/5.0211276

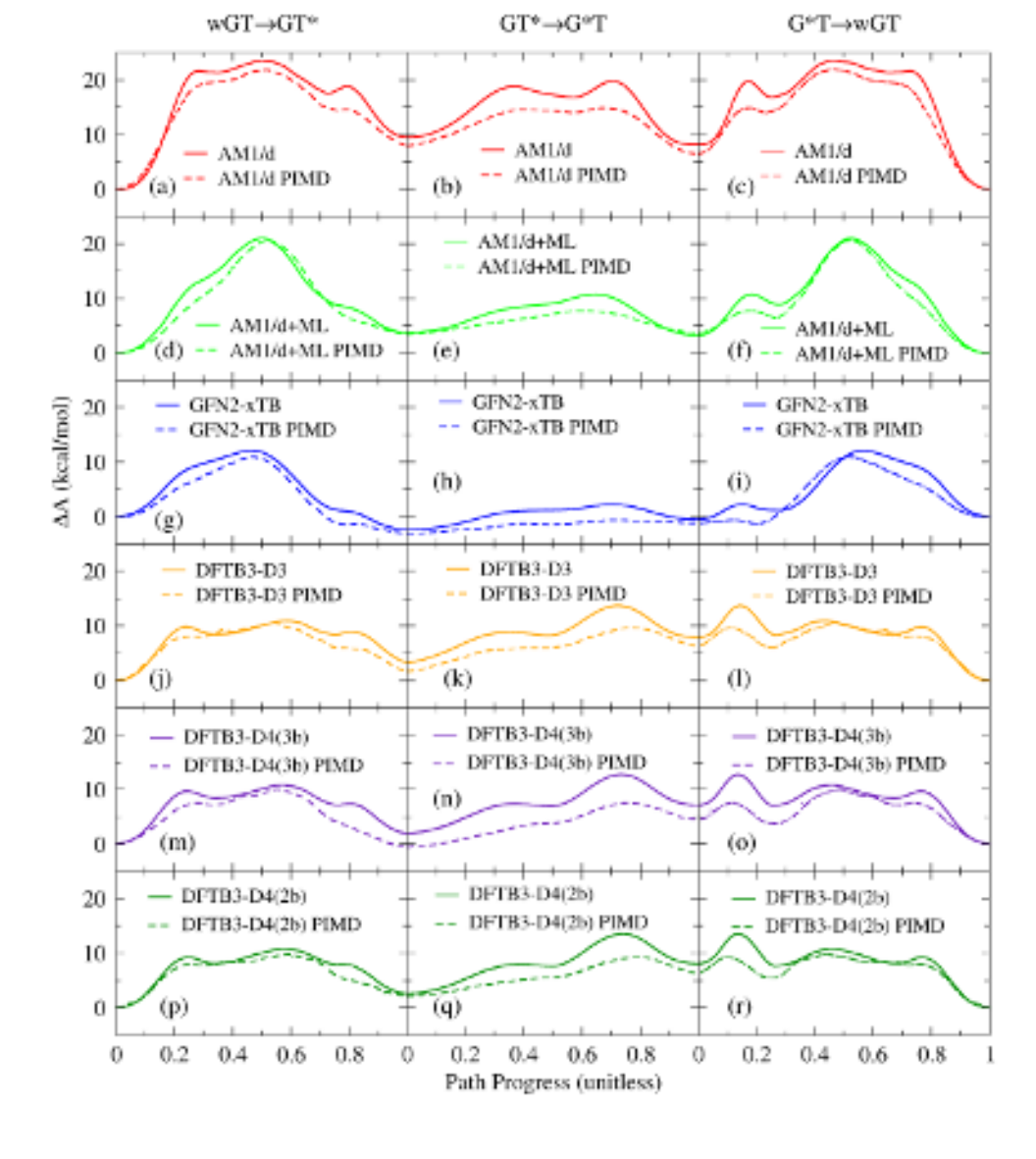


Figure 4: Classical and path-integral molecular dynamics free energy profiles for guaninethymine mispair tautomerization reactions using different semiempirical/DFTB QM/MM and QM/MM- Δ MLP models described in the text: (a) wGT \rightarrow GT* (a,d,g,j,m,p); (b) $GT^* \rightarrow G^*T$ (b,e,h,k,n,q); (c) $G^*T \rightarrow wGT$ (c,f,i,l,o,r). Here "wGT" indicates a G-T wobble pair, and G* and T* are non-standard tautomer states of G and T, respectively. Profiles from classical and PIMD are shown as solid and dashed lines, respectively. Color schemes for different models are the same as for those shown in Figure 3.

PLEASE CITE THIS ARTICLE AS DOI: 10.1063/5.0211276

works have addressed the issue of computational cost in PIMD simulations using fast density-functional tight-binding models 100 or machine learning potentials 10 optimized to high-level reference data.

Figure 4 compares the classical (solid lines) and path-integral molecular dynamics (dashed lines) free energy profiles for different semiempirical/DFTB QM/MM and QM/MM- Δ MLP models. Table 2 (bottom) lists values of key stationary points along the free energy profiles calculated with PIMD shown in Figure 4 and compares them to corresponding classical and experimentally-derived reference values. Table S2 summarizes differences between classical and PIMD free energy values. Overall, the inclusion of nuclear quantum effects generally lowers the free energy barrier (ΔA^{\ddagger}) for proton transfer steps, in some cases exceeding 3 kcal/mol, whereas the effect on ΔA is variable (ranging up to roughly ± 2.5 kcal/mol). The PIMD free energy profiles were calculated from the ring polymer centroid positions. These profiles generally have lower barriers than those produced from classical molecular dynamics. The apparent smoothing of the profile is due to the delocalization of the nuclear wave packet, which can partially be attributed to tunneling effects. ^{101–103} The current demonstration examines differences between independently-calculated free energy profiles; however, other applications of i-PI can directly evaluate equilibrium and kinetic isotope effects from umbrella sampling using thermodynamic perturbation and frequency factors. ^{21,104}

The main point of this section is to demonstrate that inclusion of nuclear quantum effects can have important quantitative effects on the free energy profiles and ΔA^{\ddagger} values for the tautomerization reactions considered here. These calculations are made practical in Amber with fast semiempirical/DFTB QM/MM and QM/MM- Δ MLP models, and enabled by the interface with i-PI. ⁴⁶

Performance

We measured the performance of the B-DNA microcanonical QM/MM simulations shown in Fig. 2 on a single Intel Xeon E5-2630 v3 CPU core clocked at 2.40 GHz. Table 3 expresses

PLEASE CITE THIS ARTICLE AS DOI: 10.1063/5.0211276

the performance as the number of classical molecular dynamics time steps per day. For example, 1,000 steps/day would correspond to 1 ps/day of sampling using a 1 fs time step. More efficient sampling with a longer integration time step may be obtained by using the "middle" thermostat scheme described in Refs. 105 and 106 in conjunction with hydrogen mass repartitioning. 107 The "QM/MM Ewald" timings use 10 Å real-space cutoffs, whereas the "QM/MM Cutoff" timings truncate the QM/MM interactions at 14 Å. The subheadings "Linked" and "File-based" refer to the communication between Sander and the QM program: Linked means there is direct communication via function calls, whereas File-based relies on disk input/output and system calls.

Table 3: Classical molecular dynamics performance using Sander with several QM/MM potentials. The values are time steps/day.

| Potential | QM/MM Ewald | QM/MM Cutoff | QM/MM Cutoff |
|--------------------------------|-------------|--------------|--------------|
| | Linked | Linked | File-based |
| DFTB3-D3 | 163,000 | 99,000 | 80,000 |
| GFN2-xTB | 133,000 | 88,000 | 80,000 |
| $\mathrm{AM1/d}$ | 133,000 | 86,000 | • • • |
| $\mathrm{AM1/d}{+}\mathrm{ML}$ | 66,000 | 51,000 | • • • |
| PBE0/6-31G* | 200 | • • • | • • • |

Table 3 suggests that linking the semiempirical programs into the Sander executable increases the performance by 10%-to-20% over file-based communication. Direct linkage further improves the performance by enabling the use of the QM/MM Ewald method, which achieves stable dynamics with smaller real-space cutoffs. The single core performance of AM1/d, GFN2-xTB, and DFTB3-D3 are very similar. The inclusion of the DPRc Δ MLP halves the AM1/d performance; however, previous examination of DPRc timings found that it decreases the performance by only 10% when the ΔMLP is evaluated on an Nvidia V100 GPU. The AM1/d+ML performance on a single CPU core is 300 times faster than PBE0/6-31G* QM/MM evaluation using the HFDF ab initio program.

The high cost of ab initio QM/MM evaluation often prevents its use within PIMD simulations. To illustrate the cost of PIMD simulations, we measured the performance of the

PLEASE CITE THIS ARTICLE AS DOI: 10.1063/5.0211276

Table 4: AM1/d QM/MM path integral molecular dynamics performance using i-PI and multiple Sander instances. N is the number of Sander instances. The path integral dynamics is propagated with 6 beads.

| N | steps/day |
|---|-----------|
| 1 | 17,000 |
| 2 | 27,000 |
| 3 | 37,000 |
| 4 | 37,000 |
| 5 | 37,000 |
| 6 | 60,000 |

wGT reactant state discussed in the previous section. The PIMD simulations were run with 6 beads; therefore, a pool of up to 6 Sander instances can be launched. Table 4 reports the simulation performance as the number of PIMD time steps evaluated per day. The total number of CPU cores is N+1, where N is the number of Sander instances; the additional core is reserved for the i-PI dynamics program. At each time step, 6 potential energy evaluations are required for the corresponding set of 6 beads; therefore, running 4 or 5 Sander instances does not improve the 3-instance performance because they are not divisors of the number of beads. When 6 instances are used, the performance is about half of what is obtained during classical dynamics due to the communication between i-PI and the Sander instances.

Conclusion

We reported new integrated software infrastructure for conducting free energy simulations in the condensed phase under periodic boundary conditions with long-ranged PME/Ewald electrostatics using a wide range of fast QM/MM potentials made available through interfaces with DFTB+ and xTB. Further, integration with DeePMD-kit enables new QM/MM-ΔMLP models to be developed and efficiently applied. Nuclear quantum effects (beyond the harmonic approximation) can be treated using free energy surface sampling with path integral molecular dynamics. The software infrastructure reported here extends the capabilities of Amber for developing new QM/MM- Δ MLP models and using them to compute free en-

PLEASE CITE THIS ARTICLE AS DOI: 10.1063/5.0211276

ergy surfaces and related properties for a wide range of applications. Near-future directions for development will involve expanding the scope of interoperability to include interfaces with enhanced sampling software, and in particular with WESTPA, ^{49,50} a scalable software package for high-performance weighted ensemble simulation and analysis.

Supporting Information

A description of the DPRc neural network and tables of tautomeric reaction free energy differences.

Acknowledgments

The authors are grateful for the financial support provided by the National Science Foundation (CSSI Frameworks Grant No. 2209717 and 2209718). This work used supercomputer Frontera¹⁰⁸ at the Texas Advanced Computing Center (TACC) through allocation CHE20002, and supercomputer Expanse at the San Diego Supercomputer Center (SDSC) through allocation CHE190067 from the Extreme Science and Engineering Discovery Environment (XSEDE), ¹⁰⁹ which was supported by National Science Foundation grant number #1548562 and from the Advanced Cyberinfrastructure Coordination Ecosystem: Services & Support (ACCESS) program, 110 which is supported by National Science Foundation grants #2138259, #2138286, #2138307, #2137603, and #2138296.

Data Availability

Example Sander input files and the trained DPRc neural network parameter sets for the B-DNA system can be downloaded from https://gitlab.com/RutgersLBSR/LBSR_SuppInfo. We are preparing tutorials describing how to use the new software infrastructure and making them available at https://gitlab.com/RutgersLBSR/AmberTutorials.

PLEASE CITE THIS ARTICLE AS DOI: 10.1063/5.0211276

References

- (1) Chipot, C., Pohorille, A., Eds. Free Energy Calculations: Theory and Applications in Chemistry and Biology; Springer Series in Chemical Physics; Springer: New York, 2007; Vol. 86.
- (2) Giese, T. J.; York, D. M. Quantum mechanical force fields for condensed phase molecular simulations. J. Phys. Condens. Matter 2017, 29, 383002.
- (3) Lee, T.-S.; Radak, B. K.; Huang, M.; Wong, K.-Y.; York, D. M. Roadmaps through free energy landscapes calculated using the multidimensional vFEP approach. J. Chem. Theory Comput. **2014**, 10, 24–34.
- (4) Giese, T. J.; Ekesan, S.; York, D. M. Extension of the Variational Free Energy Profile and Multistate Bennett Acceptance Ratio Methods for High-Dimensional Potential of Mean Force Profile Analysis. J. Phys. Chem. A 2021, 125, 4216–4232.
- (5) van der Vaart, A.; Karplus, M. Minimum free energy pathways and free energy profiles for conformational transitions based on atomistic molecular dynamics simulations. J. Chem. Phys. 2007, 126, 164106.
- (6) Hu, H.; Lu, Z.; Parks, J. M.; Burger, S. K.; Yang, W. Quantum mechanics/molecular mechanics minimum free-energy path for accurate reaction energetics in solution and enzymes: sequential sampling and optimization on the potential of mean force surface. J. Chem. Phys. 2008, 128, 34105.
- (7) Vanden-Eijnden, E.; Venturoli, M. Revisiting the finite temperature string method for the calculation of reaction tubes and free energies. J. Chem. Phys. 2009, 130, 194103.
- (8) Zinovjev, K.; Tuñón, I. Adaptive Finite Temperature String Method in Collective Variables. J. Phys. Chem. A **2017**, 121, 9764–9772.

- (9) Giese, T. J.; Ekesan, Ş.; McCarthy, E.; Tao, Y.; York, D. M. Surface-Accelerated String Method for Locating Minimum Free Energy Paths. *J. Chem. Theory Comput.* **2024**, *20*, 2058–2073.
- (10) Li, C.; Voth, G. A. Using Machine Learning to Greatly Accelerate Path Integral <i>Ab Initio</i> Molecular Dynamics. J. Chem. Theory Comput. 2022, 18, 599–604.
- (11) Gao, J. Chapter Fourteen Enzymatic Kinetic Isotope Effects from Path-Integral Free Energy Perturbation Theory . *Methods Enzymol.* **2016**, *577*, 359–88.
- (12) Vardi-Kilshtain, A.; Nitoker, N.; Major, D. T. Nuclear quantum effects and kinetic isotope effects in enzyme reactions. *Arch. Biochem. Biophys.* **2015**, *582*, 18–27.
- (13) Hwang, J. K.; Chu, Z. T.; Yadav, A.; Warshel, A. Simulations of quantum mechanical corrections for rate constants of hydride-transfer reactions in enzymes and solutions. J. Phys. Chem. 1991, 95, 8445–8448.
- (14) Hwang, J.-K.; Warshel, A. A quantized classical path approach for calculations of quantum mechanical rate constants . *J. Phys. Chem.* **1993**, *97*, 10053–10058.
- (15) Hwang, J.-K.; Warshel, A. How important are quantum mechanical nuclear motions in enzyme catalysis? *J. Am. Chem. Soc.* **1996**, *118*, 11745–11751.
- (16) Giese, T. J.; Huang, M.; Chen, H.; York, D. M. Recent Advances toward a General Purpose Linear-Scaling Quantum Force Field. *Acc. Chem. Res.* **2014**, *47*, 2812–20.
- (17) Gao, J.; Truhlar, D. G.; Wang, Y.; Mazack, M. J.; Löffler, P.; Provorse, M. R.; Rehak, P. Explicit polarization: A quantum mechanical framework for developing next generation force fields. Acc. Chem. Res. 2014, 47, 2837–2845.
- (18) Behler, J. First Principles Neural Network Potentials for Reactive Simulations of Large Molecular and Condensed Systems. Angew. Chem. Engl. 2017, 56, 12828–12840.

- (19) Meuwly, M. Machine Learning for Chemical Reactions. Chem. Rev. 2021, 121, 10218–10239.
 (20) Zeng, J.; Giese, T. J.; Ekesan, Ş.; York, D. M. Development of Range-Corrected Deep
- (20) Zeng, J.; Giese, T. J.; Ekesan, Ş.; York, D. M. Development of Range-Corrected Deep Learning Potentials for Fast, Accurate Quantum Mechanical/Molecular Mechanical Simulations of Chemical Reactions in Solution. J. Chem. Theory Comput. 2021, 17, 6993–7009.
- (21) Giese, T. J.; Zeng, J.; Ekesan, Ş.; York, D. M. Combined QM/MM, Machine Learning Path Integral Approach to Compute Free Energy Profiles and Kinetic Isotope Effects in RNA Cleavage Reactions. J. Chem. Theory Comput. 2022, 18, 4304–4317.
- (22) Pan, X.; Yang, J.; Van, R.; Epifanovsky, E.; Ho, J.; Huang, J.; Pu, J.; Mei, Y.; Nam, K.; Shao, Y. Machine-Learning-Assisted Free Energy Simulation of Solution-Phase and Enzyme Reactions. *J. Chem. Theory Comput.* **2021**, *17*, 5745–5758.
- (23) Snyder, R.; Kim, B.; Pan, X.; Shao, Y.; Pu, J. Bridging semiempirical and *ab initio* QM/MM potentials by Gaussian process regression and its sparse variants for free energy simulation. *J. Chem. Phys.* **2023**, *159*, 054107.
- (24) Zeng, J.; Tao, Y.; Giese, T. J.; York, D. M. $QD\pi$: A Quantum Deep Potential Interaction Model for Drug Discovery. *J. Chem. Theory Comput.* **2023**, *19*, 1261–1275.
- (25) Zeng, J.; Tao, Y.; Giese, T. J.; York, D. M. Modern semiempirical electronic structure methods and machine learning potentials for drug discovery: Conformers, tautomers, and protonation states. *J. Chem. Phys.* **2023**, *158*, 124110.
- (26) Han, Y.; Wang, Z.; Wei, Z.; Liu, J.; Li, J. Machine learning builds full-QM precision protein force fields in seconds. *Brief. Bioinform.* **2021**, *22*, 1–10.
- (27) Zhang, Y.-J.; Khorshidi, A.; Kastlunger, G.; Peterson, A. A. The potential for machine learning in hybrid QM/MM calculations. *J. Chem. Phys.* **2018**, *148*, 241740.

- (28) Böselt, L.; Thürlemann, M.; Riniker, S. Machine Learning in QM/MM Molecular Dynamics Simulations of Condensed- Phase Systems. *J. Chem. Theory Comput.* **2021**, 17, 2641–2658.
- (29) Shen, L.; Wu, J.; Yang, W. Multiscale Quantum Mechanics/Molecular Mechanics Simulations with Neural Networks. *J. Chem. Theory Comput.* **2016**, *12*, 4934–4946.
- (30) Shen, L.; Yang, W. Molecular Dynamics Simulations with Quantum Mechanics/Molecular Mechanics and Adaptive Neural Networks. J. Chem. Theory Comput. 2018, 14, 1442–1455.
- (31) Case, D. A.; Aktulga, H. M.; Belfon, K.; Cerutti, D. S.; Cisneros, G. A.; Cruzeiro, V. W. D.; Forouzesh, N.; Giese, T. J.; Götz, A. W.; Gohlke, H.; Izadi, S.; Kasavajhala, K.; Kaymak, M. C.; King, E.; Kurtzman, T.; Lee, T.-S.; Li, P.; Liu, J.; Luchko, T.; Luo, R.; Manathunga, M.; Machado, M. R.; Nguyen, H. M.; O'Hearn, K. A.; Onufriev, A. V.; Pan, F.; Pantano, S.; Qi, R.; Rahnamoun, A.; Risheh, A.; Schott-Verdugo, S.; Shajan, A.; Swails, J.; Wang, J.; Wei, H.; Wu, X.; Wu, Y.; Zhang, S.; Zhao, S.; Zhu, Q.; Cheatham 3rd, T. E.; Roe, D. R.; Roitberg, A.; Simmerling, C.; York, D. M.; Nagan, M. C.; Merz Jr, K. M. AmberTools. *J. Chem. Inf. Model.* 2023, 63, 6183–6191.
- (32) Cruzeiro, V. W. D.; Manathunga, M.; Merz Jr, K. M.; Götz, A. W. Open-Source Multi-GPU-Accelerated QM/MM Simulations with AMBER and QUICK. J. Chem. Inf. Model. 2021, 61, 2109–2115.
- (33) Miao, Y.; Merz Jr, K. M. Acceleration of High Angular Momentum Electron Repulsion Integrals and Integral Derivatives on Graphics Processing Units. J. Chem. Theory Comput. 2015, 11, 1449–62.
- (34) Manathunga, M.; Miao, Y.; Mu, D.; Götz, A. W.; Merz Jr, K. M. Parallel Implementation of Density Functional Theory Methods in the Quantum Interaction Computational Kernel Program. J. Chem. Theory Comput. 2020, 16, 4315–4326.

- (35) Manathunga, M.; Jin, C.; Cruzeiro, V. W. D.; Miao, Y.; Mu, D.; Arumugam, K.; Keipert, K.; Aktulga, H. M.; Merz Jr, K. M.; Götz, A. W. Harnessing the Power of Multi-GPU Acceleration into the Quantum Interaction Computational Kernel Program. J. Chem. Theory Comput. 2021, 17, 3955–3966.
- (36) Manathunga, M.; Aktulga, H. M.; Götz, A. W.; Merz Jr, K. M. Quantum Mechanics/Molecular Mechanics Simulations on NVIDIA and AMD Graphics Processing Units. J. Chem. Inf. Model. 2023, 63, 711–717.
- (37) Giese, T. J.; York, D. M. Ambient-Potential Composite Ewald Method for *ab Initio* Quantum Mechanical/Molecular Mechanical Molecular Dynamics Simulation. *J. Chem. Theory Comput.* **2016**, *12*, 2611–2632.
- (38) Bannwarth, C.; Caldeweyher, E.; Ehlert, S.; Hansen, A.; Pracht, P.; Seibert, J.; Spicher, S.; Grimme, S. Extended tight-binding quantum chemistry methods. *WIREs Comput. Mol. Sci.* **2020**, *11*, e01493.
- (39) Grimme, S.; Bannwarth, C.; Shushkov, P. A Robust and Accurate Tight-Binding Quantum Chemical Method for Structures, Vibrational Frequencies, and Noncovalent Interactions of Large Molecular Systems Parametrized for All spd-Block Elements (Z = 1–86). J. Chem. Theory Comput. 2017, 13, 1989–2009.
- (40) Grimme, S.; Bannwarth, C.; Caldeweyher, E.; Pisarek, J.; Hansen, A. A general intermolecular force field based on tight-binding quantum chemical calculations. J. Chem. Phys. 2017, 147, 161708.
- (41) Bannwarth, C.; Ehlert, S.; Grimme, S. GFN2-xTB—An Accurate and Broadly Parametrized Self- Consistent Tight-Binding Quantum Chemical Method with Multipole Electrostatics and Density-Dependent Dispersion Contributions. J. Chem. Theory Comput. 2019, 15, 1652–1671.

- (42) Hourahine, B.; Aradi, B.; Blum, V.; Bonafe, F.; Buccheri, A.; Camacho, C.; Cevallos, C.; Deshaye, M. Y.; Dumitrica, T.; Dominguez, A.; Ehlert, S.; Elstner, M.; van der Heide, T.; Hermann, J.; Irle, S.; Kranz, J. J.; Kohler, C.; Kowalczyk, T.; Kubar, T.; Lee, I. S.; Lutsker, V.; Maurer, R. J.; Min, S. K.; Mitchell, I.; Negre, C.; Niehaus, T. A.; Niklasson, A. M. N.; Page, A. J.; Pecchia, A.; Penazzi, G.; Persson, M. P.; Rezac, J.; Sanchez, C. G.; Sternberg, M.; Stohr, M.; Stuckenberg, F.; Tkatchenko, A.; z. Yu, V. W.; Frauenheim, T. DFTB+, a software package for efficient approximate density functional theory based atomistic simulations. J. Chem. Phys. 2020, 152, 124101.
- (43) Wang, H.; Zhang, L.; Han, J.; E, W. DeePMD-kit: A deep learning package for many-body potential energy representation and molecular dynamics. *Comput. Phys. Commun.* 2018, 228, 178–184.
- (44) Liang, W.; Zeng, J.; York, D. M.; Zhang, L.; Wang, H. In A Practical Guide to Recent Advances in Multiscale Modeling and Simulation of Biomolecules; Wang, Y., Zhou, R., Eds.; AIP Publishing, 2023; Chapter Chapter 6, pp 6–1–6–20.
- (45) Zeng, J.; Zhang, D.; Lu, D.; Mo, P.; Li, Z.; Chen, Y.; Rynik, M.; Huang, L.; Li, Z.; Shi, S.; Wang, Y.; Ye, H.; Tuo, P.; Yang, J.; Ding, Y.; Li, Y.; Tisi, D.; Zeng, Q.; Bao, H.; Xia, Y.; Huang, J.; Muraoka, K.; Wang, Y.; Chang, J.; Yuan, F.; Bore, S. L.; Cai, C.; Lin, Y.; Wang, B.; Xu, J.; Zhu, J.-X.; Luo, C.; Zhang, Y.; Goodall, R. E. A.; Liang, W.; Singh, A. K.; Yao, S.; Zhang, J.; Wentzcovitch, R.; Han, J.; Liu, J.; Jia, W.; York, D. M.; E, W.; Car, R.; Zhang, L.; Wang, H. DeePMD-kit v2: A software package for deep potential models. J. Chem. Phys. 2023, 159, 054801.
- (46) Kapil, V.; Rossi, M.; Marsalek, O.; Petraglia, R.; Litman, Y.; Spura, T.; Cheng, B.; Cuzzocrea, A.; Meißner, R. H.; Wilkins, D. M.; Helfrecht, B. A.; Juda, P.; Bienvenue, S. P.; Fang, W.; Kessler, J.; Poltavsky, I.; Vandenbrande, S.; Wieme, J.; Corminboeuf, C.; Kühne, T. D.; Manolopoulos, D. E.; Markland, T. E.; Richardson, J. O.;

- Tkatchenko, A.; Tribello, G. A.; Van Speybroeck, V.; Ceriotti, M. i-PI 2.0: A universal force engine for advanced molecular simulations. *Comput. Phys. Commun.* **2019**, *236*, 214–223.
- (47) Bonomi, M.; Branduardi, D.; Bussi, G.; Camilloni, C.; Provasi, D.; Raiteri, P.; Donadio, D.; Marinelli, F.; Pietrucci, F.; Broglia, R.; Parrinello, M. PLUMED: a portable plugin for free energy calculations with molecular dynamics. *Comput. Phys. Commun.* **2009**, *180*, 1961–1972.
- (48) Tribello, G. A.; Bonomi, M.; Branduardi, D.; Camilloni, C.; Bussi, G. PLUMED2: New feathers for an old bird. *Comput. Phys. Commun.* **2014**, *185*, 604–613.
- (49) Zwier, M. C.; Adelman, J. L.; Kaus, J. W.; Pratt, A. J.; Wong, K. F.; Rego, N. B.; Suárez, E.; Lettieri, S.; Wang, D. W.; Grabe, M.; Zuckerman, D. M.; Chong, L. T. WESTPA: An Interoperable, Highly Scalable Software Package for Weighted Ensemble Simulation and Analysis. J. Chem. Theory Comput. 2015, 11, 800–809.
- (50) Russo, J. D.; Zhang, S.; Leung, J. M. G.; Bogetti, A. T.; Thompson, J. P.; De-Grave, A. J.; Torrillo, P. A.; Pratt, A. J.; Wong, K. F.; Xia, J.; Copperman, J.; Adelman, J. L.; Zwier, M. C.; LeBard, D. N.; Zuckerman, D. M.; Chong, L. T. WESTPA 2.0: High-Performance Upgrades for Weighted Ensemble Simulations and Analysis of Longer-Timescale Applications. J. Chem. Theory Comput. 2022, 18, 638–649.
- (51) Giese, T. J.; York, D. M. FE-ToolKit: The free energy analysis toolkit. https://gitlab.com/RutgersLBSR/fe-toolkit, Accessed: March 3, 2024.
- (52) Nam, K.; Gao, J.; York, D. M. An efficient linear-scaling Ewald method for long-range electrostatic interactions in combined QM/MM calculations. J. Chem. Theory Comput. 2005, 1, 2–13.
- (53) Giese, T. J.; Panteva, M. T.; Chen, H.; York, D. M. Multipolar Ewald methods, 1: Theory, accuracy, and performance. *J. Chem. Theory Comput.* **2015**, *11*, 436–450.

- (54) Giese, T. J.; Panteva, M. T.; Chen, H.; York, D. M. Multipolar Ewald methods, 2: Applications using a quantum mechanical force field. J. Chem. Theory Comput. 2015, 11, 451–461.
- (55) Kimsey, I. J.; Szymanski, E. S.; Zahurancik, W. J.; Shakya, A.; Xue, Y.; Chu, C.-C.; Sathyamoorthy, B. J.; Suo, Z.; Al-Hashimi, H. M. Dynamic basis for dG.dT misincorporation via tautomerization and ionization. *Nature* **2018**, *554*, 195–201.
- (56) Li, P.; Rangadurai, A.; Al-Hashimi, H. M.; Hammes-Schiffer, S. Environmental Effects on Guanine-Thymine Mispair Tautomerization Explored with Quantum Mechanical/Molecular Mechanical Free Energy Simulations. J. Am. Chem. Soc. 2020, 142, 11183–11191.
- (57) Hourahine, B.; Aradi, B.; Blum, V.; Bonafé, F.; Buccheri, A.; Camacho, C.; Cevallos, C.; Deshaye, M. Y.; Dumitrică, T.; Dominguez, A.; Ehlert, S.; Elstner, M.; van der Heide, T.; Hermann, J.; Irle, S.; Kranz, J. J.; Köhler, C.; Kowalczyk, T.; Kubař, T.; Lee, I. S.; Lutsker, V.; Maurer, R. J.; Min, S. K.; Mitchell, I.; Negre, C.; Niehaus, T. A.; Niklasson, A. M. N.; Page, A. J.; Pecchia, A.; Penazzi, G.; Persson, M. P.; Řezáč, J.; Sánchez, C. G.; Sternberg, M.; Stöhr, M.; Stuckenberg, F.; Tkatchenko, A.; Yu, V. W.-z.; Frauenheim, T. DFTB+: general package for performing fast atomistic calculations. https://github.com/dftbplus/dftbplus, Accessed: March 3, 2024.
- (58) Bannwarth, C.; Caldeweyher, E.; Ehlert, S.; Hansen, A.; Pracht, P.; Seibert, J.; Spicher, S.; Grimme, S. Semiempirical extended tight-binding program package. https://github.com/grimme-lab/xtb, Accessed: March 3, 2024.
- (59) Darden, T.; York, D.; Pedersen, L. Particle mesh Ewald: An N log(N) method for Ewald sums in large systems. J. Chem. Phys. 1993, 98, 10089–10092.
- (60) Essmann, U.; Perera, L.; Berkowitz, M. L.; Darden, T.; Lee, H.; Pedersen, L. G. A smooth particle mesh Ewald method. *J. Chem. Phys.* **1995**, *103*, 8577–8593.

accepted manuscript. However, the online version of record will be different from this version once it has been copyedited and typeset

PLEASE CITE THIS ARTICLE AS DOI: 10.1063/5.0211276

This is the author's peer reviewed,

- (61) Dral, P. O.; Zubatiuk, T.; Xue, B.-X. In Quantum Chemistry in the Age of Machine Learning; Dral, P. O., Ed.; Elsevier, 2022; Chapter 21, pp 491–507.
- (62) Liu, Y.; Li, J. Permutation-Invariant-Polynomial Neural-Network-Based Δ -Machine Learning Approach: A Case for the HO₂ Self-Reaction and Its Dynamics Study. J. Phys. Chem. Lett. **2022**, 13, 4729–4738.
- (63) Ruth, M.; Gerbig, D.; Schreiner, P. R. Machine Learning of Coupled Cluster (T)-Energy Corrections via Delta (Δ)-Learning. J. Chem. Theory Comput. 2022, 18, 4846–4855.
- (64) Unzueta, P. A.; Greenwell, C. S.; Beran, G. J. O. Predicting Density Functional Theory-Quality Nuclear Magnetic Resonance Chemical Shifts via Δ -Machine Learning. J. Chem. Theory Comput. **2021**, 17, 826–840.
- (65) Musaelian, A.; Batzner, S.; Johansson, A.; Sun, L.; Owen, C. J.; Kornbluth, M.; Kozinsky, B. Learning local equivariant representations for large-scale atomistic dynamics. Nat. Commun. 2023, 14, 579.
- (66) Batatia, I.; Kovacs, D. P.; Simm, G. N. C.; Ortner, C.; Csanyi, G. MACE: Higher Order Equivariant Message Passing Neural Networks for Fast and Accurate Force Fields. 2022; https://openreview.net/forum?id=YPpSngE-ZU.
- (67) Ansel, J.; Yang, E.; He, H.; Gimelshein, N.; Jain, A.; Voznesensky, M.; Bao, B.; Bell, P.; Berard, D.; Burovski, E.; Chauhan, G.; Chourdia, A.; Constable, W.; Desmaison, A.; DeVito, Z.; Ellison, E.; Feng, W.; Gong, J.; Gschwind, M.; Hirsh, B.; Huang, S.; Kalambarkar, K.; Kirsch, L.; Lazos, M.; Lezcano, M.; Liang, Y.; Liang, J.; Lu, Y.; Luk, C. K.; Maher, B.; Pan, Y.; Puhrsch, C.; Reso, M.; Saroufim, M.; Siraichi, M. Y.; Suk, H.; Zhang, S.; Suo, M.; Tillet, P.; Zhao, X.; Wang, E.; Zhou, K.; Zou, R.; Wang, X.; Mathews, A.; Wen, W.; Chanan, G.; Wu, P.; Chintala, S. PyTorch

- 2: Faster Machine Learning Through Dynamic Python Bytecode Transformation and Graph Compilation. 2024; https://doi.org/10.1145/3620665.3640366.
- (68) Ceriotti, M.; More, J.; Manolopoulos, D. E. i-PI: A Python interface for ab initio path integral molecular dynamics simulations. *Comput. Phys. Commun.* **2014**, *185*, 1019–1026.
- (69) Ceriotti, M.; Manolopoulos, D. E. Efficient first-principles calculation of the quantum kinetic energy and momentum distribution of nuclei. *Phys. Rev. Lett.* 2012, 109, 100604.
- (70) Ceriotti, M.; Markland, T. E. Efficient methods and practical guidelines for simulating isotope effects. *J. Chem. Phys.* **2013**, *138*, 014112.
- (71) Hunter, W. N.; Brown, T.; Kneale, G.; Anand, N. N.; Rabinovich, D.; Kennard, O. The Structure of Guanosine-Thymidine Mismatches in B-DNA at 2.5 Angstroms Resolution. *J. Biol. Chem.* **1993**, *262*, 9962–9970.
- (72) Kimsey, I. J.; Petzold, K.; Sathyamoorthy, B.; Stein, Z. W.; Al-Hashimi, H. M. Visualizing transient Watson–Crick-like mispairs in DNA and RNA duplexes. *Nature* **2015**, 519, 315–320.
- (73) Szymanski, E. S.; Kimsey, I. J.; Al-Hashimi, H. M. Direct NMR Evidence that Transient Tautomeric and Anionic States in dG·dT Form Watson–Crick-like Base Pairs. *J. Am. Chem. Soc.* **2017**, *139*, 4326–4329.
- (74) Wang, W.; Hellinga, H. W.; Beese, L. S. Structural evidence for the rare tautomer hypothesis of spontaneous mutagenesis. Proc. Natl. Acad. Sci. U. S. A. 2011, 108, 17644–8.
- (75) Bebenek, K.; Pedersen, L. C.; Kunkel, T. A. Replication infidelity via a mismatch with Watson–Crick geometry. *Proc. Natl. Acad. Sci. USA* **2011**, *108*, 1862–1867.

- (76) Rozov, A.; Demeshkina, N.; Westhof, E.; Yusupov, M.; Yusupova, G. New Structural Insights into Translational Miscoding. Trends Biochem. Sci. 2016, 41, 798–814.
- (77) Ekesan, S.; York, D. M. Dynamical ensemble of the active state and transition state mimic for the RNA-cleaving 8-17 DNAzyme in solution. Nucleic Acids Res. 2019, 47, 10282 - 10295.
- (78) Loncharich, R. J.; Brooks, B. R.; Pastor, R. W. Langevin dynamics of peptides: the frictional dependence of isomerization rates of N-acetylalanyl-N'-methylamide. Biopolymers 1992, 32, 523–535.
- (79) Galindo-Murillo, R.; Robertson, J. C.; Zgarbova, M.; Sponer, J.; Otyepka, M.; Jurecka, P.; Cheatham III, T. E. Assessing the current state of AMBER force field modifications for DNA. J. Chem. Theory Comput. 2016, 12, 4114–4127.
- (80) Wu, Y.: Tepper, H. L.: Voth, G. A. Flexible simple point-charge water model with improved liquid-state properties. J. Chem. Phys. 2006, 124, 024503.
- (81) Li, P.; Roberts, B. P.; Chakravorty, D. K.; Merz, Jr., K. M. Rational design of Particle Mesh Ewald compatible Lennard-Jones parameters for +2 metal cations in explicit solvent. J. Chem. Theory Comput. **2013**, 9, 2733–2748.
- (82) Dewar, M. J. S.; Zoebisch, E.; Healy, E. F.; Stewart, J. J. P. Development and use of quantum mechanical molecular models. 76. AM1: a new general purpose quantum mechanical molecular model. J. Am. Chem. Soc. 1985, 107, 3902–3909.
- (83) Lopez, X.; York, D. M. Parameterization of semiempirical methods to treat nucleophilic attacks to biological phosphates: AM1/d parameters for phosphorus. Theor. Chem. Acc. 2003, 109, 149–159.
- (84) Nam, K.; Cui, Q.; Gao, J.; York, D. M. Specific reaction parametrization of the AM1/d

- Hamiltonian for phosphoryl transfer reactions: H, O, and P atoms. J. Chem. Theory Comput. 2007, 3, 486–504.
- (85) Grimme, S.; Antony, J.; Ehrlich, S.; Krieg, H. A consistent and accurate ab initio parametrization of density functional dispersion correction (DFT-D) for the 94 elements H-Pu. J. Chem. Phys. **2010**, 132, 154104–154123.
- (86) Grimme, S.; Ehrlich, S.; Goerigk, L. Effect of the damping function in dispersion corrected density functional theory. *J. Comput. Chem.* **2011**, *32*, 1456–1465.
- (87) Gaus, M.; Goez, A.; Elstner, M. Parametrization and Benchmark of DFTB3 for Organic Molecules. J. Chem. Theory Comput. **2013**, 9, 338–354.
- (88) Gaus, M.; Lu, X.; Elstner, M.; Cui, Q. Parameterization of DFTB3/3OB for Sulfur and Phosphorus for Chemical and Biological Applications. J. Chem. Theory Comput. 2014, 10, 1518–1537.
- (89) Caldeweyher, E.; Ehlert, S.; Hansen, A.; Neugebauer, H.; Spicher, S.; Bannwarth, C.; Grimme, S. A generally applicable atomic-charge dependent London dispersion correction. *J. Chem. Phys.* **2019**, *150*, 154122.
- (90) Shirts, M. R.; Chodera, J. D. Statistically optimal analysis of samples from multiple equilibrium states. *J. Chem. Phys.* **2008**, *129*, 124105.
- (91) Ceriotti, M.; Manolopoulos, D. E.; Parrinello, M. Accelerating the convergence of path integral dynamics with a generalized Langevin equation. J. Chem. Phys. 2011, 134, 084104.
- (92) Ceriotti, M.; Bussi, G.; Parrinello, M. Colored-Noise Thermostats à la Carte. *J. Chem. Theory Comput.* **2010**, *6*, 1170–1180.
- (93) Ceriotti, M.; Bussi, G.; Parrinello, M. Langevin Equation with Colored Noise for

- Constant-Temperature Molecular Dynamics Simulations. Phys. Rev. Lett. 2009, 102, 020601.
- (94) Giese, T. J.; Zeng, J.; York, D. M. Multireference Generalization of the Weighted Thermodynamic Perturbation Method. J. Phys. Chem. A 2022, 126, 8519–8533.
- (95) Zhang, Y.; Wang, H.; Chen, W.; Zeng, J.; Zhang, L.; Han, W.; E, W. DP-GEN: A concurrent learning platform for the generation of reliable deep learning based potential energy models. Comput. Phys. Commun. 2020, 253, 107206.
- (96) Kingma, D. P.; Ba, J. Adam: A Method for Stochastic Optimization. 2017,
- (97) Nishimoto, K.; Mataga, N. Electronic structure and spectra of some nitrogen heterocycles. Z. Phys. Chem. 1957, 12, 335–338.
- (98) Ohno, K. Some remarks on the Pariser-Parr-Pople method. Theor. Chim. Act. 1964, 2, 219–227.
- (99) Klopman, G. A semiempirical treatment of molecular structures, II. Molecular terms and application to diatomic molecules. J. Am. Chem. Soc. 1964, 86, 4550–4557.
- (100) Kosugi, K.; Nakano, H.; Sato, H. SCC-DFTB-PIMD Method To Evaluate a Multidimensional Quantum Free-Energy Surface for a Proton-Transfer Reaction. J. Chem. Theory Comput. 2019, 15, 4965–4973.
- (101) Tuckerman, M. E. Statistical Mechanics: Theory and Molecular Simulation; Oxford University Press, 2010.
- (102) Cendagorta, J. R.; Shen, H.; Bačić, Z.; Tuckerman, M. E. Enhanced Sampling Path Integral Methods Using Neural Network Potential Energy Surfaces with Application to Diffusion in Hydrogen Hydrates. Adv. Theory Simul. 2021, 4, 2000258.

- (103) Lamaire, A.; Cools-Ceuppens, M.; Bocus, M.; Verstraelen, T.; Van Speybroeck, V. Quantum Free Energy Profiles for Molecular Proton Transfers. *J. Chem. Theory Comput.* **2023**, *19*, 18–24.
- (104) Giese, T. J.; York, D. M. Estimation of frequency factors for the calculation of kinetic isotope effects from classical and path integral free energy simulations. J. Chem. Phys. 2023, 158, 174105–174115.
- (105) Zhang, Z.; Liu, X.; Chen, Z.; Zheng, H.; Yan, K.; Liu, J. A unified thermostat scheme for efficient configurational sampling for classical/quantum canonical ensembles via molecular dynamics. J. Chem. Phys. 2017, 147, 034109.
- (106) Zhang, Z.; Liu, X.; Yan, K.; Tuckerman, M. E.; Liu, J. Unified Efficient Thermostat Scheme for the Canonical Ensemble with Holonomic or Isokinetic Constraints via Molecular Dynamics. *J. Phys. Chem. A* **2019**, *123*, 6056–6079.
- (107) Hopkins, C. W.; Le Grand, S.; Walker, R. C.; Roitberg, A. E. Long-Time-Step Molecular Dynamics through Hydrogen Mass Repartitioning. *J. Chem. Theory Comput.* **2015**, *11*, 1864–1874.
- (108) Stanzione, D.; West, J.; Evans, R. T.; Minyard, T.; Ghattas, O.; Panda, D. K. PEARC'20: Practice and Experience in Advanced Research Computing; Frontera: The Evolution of Leadership Computing at the National Science Foundation; Association for Computing Machinery, 2020; pp 106–111.
- (109) Towns, J.; Cockerill, T.; Dahan, M.; Foster, I.; Gaither, K.; Grimshaw, A.; Hazlewood, V.; Lathrop, S.; Lifka, D.; Peterson, G. D.; Roskies, R.; Scott, J. R.; Wilkins-Diehr, N. XSEDE: Accelerating Scientific Discovery. Comput. Sci. Eng. 2014, 16, 62–74.
- (110) Boerner, T. J.; Deems, S.; Furlani, T. R.; Knuth, S. L.; Towns, J. In *PEARC'23: Practice and Experience in Advanced Research Computing*; Romanella, R. S. A., Knuth, S.,

This is the author's peer reviewed, accepted manuscript. However, the online version of record will be different from this version once it has been copyedited and typeset.

PLEASE CITE THIS ARTICLE AS DOI: 10.1063/5.0211276

Cyberinfrastructure Coordination Ecosystem: Services & Supports; Association for Computing Machinery, 2023; pp 173–176.

Hackworth, K., Pummill, J., Eds.; ACCESS: Advancing Innovation: NSF's Advanced

41